Katanin controls mitotic and meiotic spindle length

Karen McNally,[1] Anjon Audhya,[2] Karen Oegema,[2] and Francis J. McNally[1]

[1]Section of Molecular and Cellular Biology, University of California, Davis, Davis, CA 95616
[2]Department of Cellular and Molecular Medicine, Ludwig Institute for Cancer Research, University of California, San Diego, La Jolla, CA 92093

Accurate control of spindle length is a conserved feature of eukaryotic cell division. Lengthening of mitotic spindles contributes to chromosome segregation and cytokinesis during mitosis in animals and fungi. In contrast, spindle shortening may contribute to conservation of egg cytoplasm during female meiosis. Katanin is a microtubule-severing enzyme that is concentrated at mitotic and meiotic spindle poles in animals. We show that inhibition of katanin slows the rate of spindle shortening in nocodazole-treated mammalian fibroblasts and in untreated *Caenorhabditis elegans* meiotic embryos. Wild-type *C. elegans* meiotic spindle shortening proceeds through an early katanin-independent phase marked by increasing microtubule density and a second, katanin-dependent phase that occurs after microtubule density stops increasing. In addition, double-mutant analysis indicated that γ-tubulin–dependent nucleation and microtubule severing may provide redundant mechanisms for increasing microtubule number during the early stages of meiotic spindle assembly.

Introduction

Control of spindle length is important for different reasons during mitotic and meiotic cell divisions. Mitotic spindles of most animals and fungi lengthen in a process called anaphase B. This spindle lengthening provides a mechanism for moving sister chromatids apart that is redundant with anaphase A. The meiotic spindles of animal oocytes, however, are different because they mediate highly asymmetric cell divisions in which chromosomes are discarded in nonviable division products called polar bodies. The female meiotic spindles of mouse do not lengthen during anaphase, and a mutation causing anaphase B–like spindle elongation results in a large polar body and a correspondingly small egg (Verlhac et al., 2000). This result indicates that restriction of meiotic spindle length may be important for preserving egg volume and egg contents required by the embryo. Indeed, the meiotic spindles of *Caenorhabditis elegans* zygotes actually shorten in a coordinated, anaphase-promoting complex-dependent manner during meiosis I and II (Yang et al., 2003, 2005).

Results published during the last 10 yr indicate that a discrete set of spindle-lengthening and spindle-shortening mechanisms can control overall spindle length. In many organisms, the plus ends of kinetochore fiber microtubules polymerize at the same rate that the minus ends depolymerize (Mitchison, 1989). When plus-end polymerization is blocked with taxol (Waters et al., 1996) or by depletion of the kinetochore protein, CLASP (CLIP170-associated protein; Maiato et al., 2005), spindles shorten because of continued minus-end depolymerization. Conversely, when minus-end depolymerization is blocked experimentally, spindles can elongate continuously (Rogers et al., 2004). In addition, *Drosophila melanogaster* spindles elongate excessively in the absence of the kinetochore-associated microtubule depolymerase, KLP67A (Gandhi et al., 2004; Goshima et al., 2005). Another major lengthening mechanism is outward sliding of overlapping antiparallel microtubules mediated by kinesin-5 family members (Sharp et al., 1999; Kapitein et al., 2005). In unperturbed *D. melanogaster* embryonic spindles, a cell cycle–regulated cessation of minus-end depolymerization coincides with the initiation of anaphase B spindle elongation. In this case, the rate of kinesin-5–driven outward sliding is matched by the rate of minus-end depolymerization until this depolymerization stops (Brust-Mascher and Scholey, 2002). Evidence has also been presented for two other spindle-shortening mechanisms, inward sliding of overlapping antiparallel microtubules by kinesin-14 family members (Mountain et al., 1999; Sharp et al., 1999) and an undefined "tensile element" that squeezes inward and buckles microtubule bundles during nocodazole-induced spindle shortening (Mitchison et al., 2005).

None of these mechanisms appear to be universally used for spindle-length control. For example, cessation of minus-end depolymerization does not alter spindle length in human U2OS cells (Ganem et al., 2005) and minus-end depolymerization does not occur at all in some fungal cells (Mallavarapu et al., 1999; Maddox et al., 2000). Separation of spindle poles occurs

Correspondence to Francis J. McNally: fjmcnally@ucdavis.edu

Abbreviations used in this paper: CCD, charge-coupled device; γ-TuRC, γ-tubulin ring complex.

The online version of this article contains supplemental material.

The Journal of Cell Biology, Vol. 175, No. 6, December 18, 2006 881–891
http://www.jcb.org/cgi/doi/10.1083/jcb.200608117

Table I. **Mean spindle-shortening velocities in nocodazole-treated CV1 cells (μm/s)**

Time after nocodazole perfusion	Untransfected (n = 9)	CFP (n = 14)	CFP-con80 (n = 11)	CFP-Ploop-p60 (n = 17)	CFP-ΔN-Ploop-P60 (n = 6)
0–35 s	.076 ± 0.026	.054 ± 0.019	.035 ± 0.014	.034 ± 0.018	.054 ± 0.026
60–140 s	.023 ± 0.010	.022 ± 0.015	.010 ± 0.005	.015 ± 0.004	.023 ± 0.010

in *C. elegans* mitotic embryos even after laser cutting of spindle microtubules (Grill et al., 2001). This outward movement of spindle poles is thought to be driven by a cortical motor protein pulling on astral microtubules that extend from the spindle pole toward the cortex. Thus, *C. elegans* mitotic spindles can "elongate" in the absence of an outward sliding mechanism. This may explain why the sole kinesin-5 in this species is not essential (Bishop et al., 2005). In contrast, budding yeast mitotic spindles can elongate in the complete absence of cortical pulling forces (Sullivan and Huffaker, 1992), and this species' kinesin-5 family members are essential (Hoyt et al., 1992).

The goal of this study was to determine whether the microtubule-severing protein, katanin, has a conserved role in spindle-length control. Katanin is a heterodimeric protein consisting of an AAA ATPase subunit called p60 and an accessory subunit called p80. The ATPase subunits from sea urchin (Hartman et al., 1998) and human (McNally et al., 2000) can sever microtubules on their own, but this activity is enhanced by the p80 subunit. Katanin's microtubule-severing activity and its conserved localization at the spindle poles of sea urchins (McNally et al., 1996) and vertebrates (McNally and Thomas, 1998) make it a strong candidate for playing a role in spindle-length control.

We previously reported that inhibition of katanin in mammalian cells causes a change in the distribution of γ-tubulin and a reduction in the rate of nocodazole-induced spindle microtubule depolymerization as assayed by decreasing fluorescence intensity of YFP-tubulin (Buster et al., 2002). Here, we report that katanin inhibition slows the rate of nocodazole-induced spindle shortening in mitotic mammalian cells and blocks the second of two meiotic spindle shortening phases in *C. elegans*.

Results

Katanin promotes spindle shortening in nocodazole-treated mammalian cells

Previous studies have demonstrated that inhibition of microtubule polymerization with taxol (Waters et al., 1996) or nocodazole (Mitchison et al., 2005) can induce mitotic spindle shortening and thus reveal spindle-shortening forces that were balanced by polymerization-dependent spindle-lengthening forces before drug treatment. To test whether katanin contributes to inward forces in the mitotic spindle, we measured the velocity of nocodazole-induced spindle shortening in cells expressing YFP-tubulin and CFP fusions to each of two katanin inhibitors. We previously found that these inhibitors slowed the rate of nocodazole-induced microtubule depolymerization as assayed by the rate of decrease in YFP-tubulin fluorescence intensity but did not quantify spindle-shortening velocities (Buster et al., 2002). Nocodazole-induced spindle shortening was biphasic with an early, fast phase and a later, slow phase. As shown in Table I, both con80, a p80 katanin fragment that displaces endogenous p60 katanin from spindle poles (McNally et al., 2000), and Ploop-p60, a point mutant of p60 katanin that inhibits the in vitro microtubule-severing activity of wild-type katanin (Buster et al., 2002), slowed both the early and late phases of nocodazole-induced spindle shortening relative to control cells expressing CFP alone. In contrast, a CFP fusion to a p60 katanin subunit that does not inhibit severing by wild-type katanin, ΔN-Ploop-p60 (Buster et al., 2002), did not slow the rate of spindle shortening relative to control cells expressing CFP alone. These results indicate that katanin-mediated microtubule severing promotes spindle shortening when polymerization is blocked. We propose that microtubule severing in untreated spindles generates arrays of short, overlapping microtubules near spindle poles. Nocodazole-mediated depolymerization would lead to a rapid loss of microtubule overlap that is required for the kinesin 5–mediated outward sliding that opposes spindle-shortening mechanisms. In the absence of microtubule-severing activity at spindle poles, microtubules would be longer, overlap zones would be longer, and more time would be required for nocodazole to cause a loss of overlap (see Discussion).

Table II. **Comparison of meiotic spindle measurements in wild-type and *mei-2(ct98)* embryos**

Measurement	Wild type	*mei-2(ct98)*
Maximum spindle length MI	7.72 ± 0.50 μm (n = 12)	9.62 ± 0.79 μm (n = 12)
Maximum spindle length MII	6.21 ± 0.35 μm (n = 12)	9.22 ± 0.82 μm (n = 8)
Minimum spindle length MI	2.77 ± 0.31 μm (n = 12)	6.19 ± 0.43 μm (n = 9)
Minimum spindle length MII	2.43 ± 0.21 μm (n = 12)	5.84 ± 0.59 μm (n = 11)
Minimum spindle length (percentage of maximum length [combined MI/MII])	37.6 ± 4.5% (n = 24)	64.6 ± 4.1% (n = 11)
Percentage of maximum length at onset of density decrease MI	57.6 ± 6% (n = 12)	64.3 ± 8% (n = 9)
Percentage of maximum length at onset of density decrease MII	63.4 ± 7% (n = 12)	63.3 ± 8% (n = 8)
Rate of shortening during density increase	−1.08 ± 0.36 μm/min (n = 12)	−0.95 ± 0.30 μm/min (n = 12)
Rate of shortening during density decrease	−0.74 ± 0.05 μm/min (n = 12)	−0.01 ± 0.08 μm/min (n = 9)
Angle of rotation	96.6 ± 4.9° (n = 18)	133.8 ± 32.4° (n = 18)
Polar body size	3.56 ± 0.62 μm^2 (n = 32)	5.04 ± 2.12 μm^2 (n = 34)

To test the generality of katanin's role in spindle-length control and to examine spindle shortening in the absence of drugs, we continued our analysis with *C. elegans* female meiotic spindles. These spindles were chosen because they are the only spindles that have well-documented and dramatic shortening phases (Yang et al., 2003) and they are the only spindles that have a demonstrated requirement for a katanin homologue, MEI-1–MEI-2 (Mains et al., 1990; Srayko et al., 2000).

Katanin promotes the second of two spindle-shortening phases during *C. elegans* female meiosis

In wild-type *C. elegans*, MI and MII spindles shorten from steady-state metaphase lengths of 7.7 and 6.2 μm, respectively, to minimum lengths of 2.8 and 2.4 μm (Yang et al., 2003; Table II and Fig. 1). After reaching minimal length, the spindles narrow and lengthen to form a midbody that extends into the polar body. As shown in Fig. 1 A, spindle shortening could occur by either of two general mechanisms, inward sliding of antiparallel microtubules or depolymerization of microtubule minus ends at spindle poles. In a sliding-only mechanism, microtubule density increases as the spindle shortens. If spindle shortening proceeded only by minus-end depolymerization or by a combination of inward sliding and plus-end depolymerization, microtubule density would not increase.

To distinguish between these possibilities, changes in microtubule density were monitored by obtaining the mean fluorescence intensity of GFP::tubulin (mean pixel value) in the spindle throughout meiosis (see Materials and methods). In the example shown in Fig. 1 B, GFP::tubulin fluorescence intensity remained constant when spindle length was constant (Fig. 1 B, 0–1.5 min) but began to increase dramatically as the spindle shortened (Fig. 1 B, 1.5–5 min). This increase in microtubule density abruptly switched to decreasing microtubule density when spindle length reached 56% of its starting metaphase length (Fig. 1 B, 5–7.5 min). The switch between increasing and decreasing microtubule density began within 1 min of spindle rotation from parallel to perpendicular relative to the cortex. We previously demonstrated that homologue separation initiates 0.7 min after spindle rotation (McNally and McNally, 2005). After the transition from increasing to decreasing density, the spindle continued to shorten to 33% of its starting length. Similar results, obtained in 12 out of 12 experiments (Table II) using wild-type *C. elegans* during either MI or MII, indicated that there are two sequential and mechanistically distinct phases of meiotic spindle shortening. The first phase most likely occurs by inward sliding of antiparallel microtubules that stops just before rotation, perhaps because at that point the microtubules are completely overlapped. Microtubule density increases uniformly in all parts of the spindle during the first phase (unpublished data), possibly because the microtubule overlap zones are heterogeneous in length and position within the spindle. The second shortening phase occurs after rotation, during chromosome segregation, and is accompanied by net microtubule depolymerization.

To test the role of microtubule severing in meiotic spindle shortening, we chose a partial-loss-of-function mutation in the p80 katanin homologue, *mei-2*, because null mutants of *mei-2* or the p60 katanin homologue, *mei-1*, do not assemble bipolar spindles (Mains et al., 1990), and failure of these spindles to shrink (Yang et al., 2003) might be an indirect result of a lack of antiparallel microtubules. The missense mutant *mei-2(ct98)* has a reduced amount of MEI-2 protein (Srayko et al., 2000). We tested the in vitro microtubule-severing activity of purified

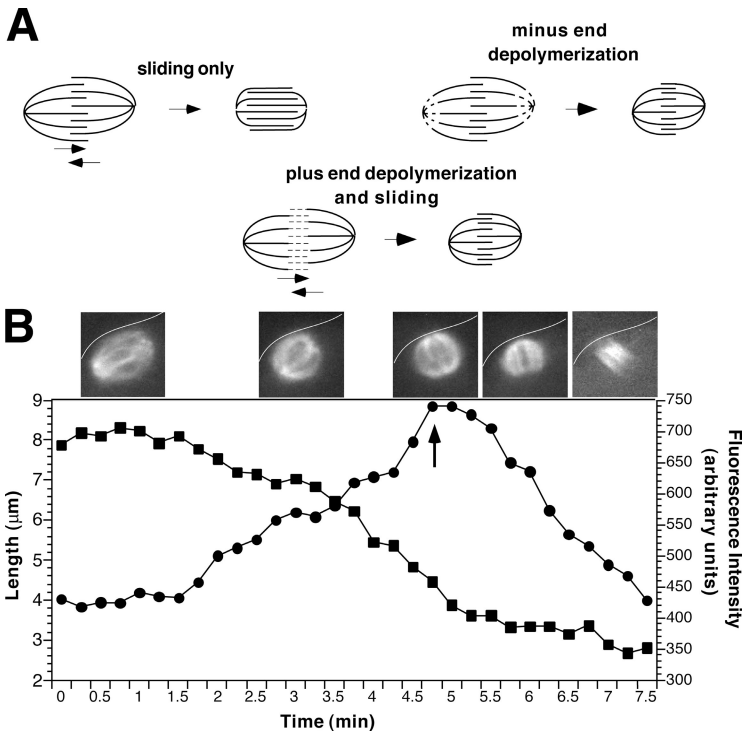

Figure 1. **Wild-type meiotic spindles shorten by two distinct, sequential mechanisms.** (A) Spindle shortening could occur by one of three mechanisms. In the "sliding only" mechanism, the spindle is shortened by minus end–directed kinesins that slide antiparallel microtubule bundles inward. In this mechanism, the density of spindle microtubules increases as the spindle shortens. In the second mechanism, microtubule minus ends are depolymerized at spindle poles. In the third mechanism, plus-end depolymerization is accompanied by inward sliding. (B) Graph of the length (squares) and fluorescence intensity (circles) of a wild-type meiotic spindle from time-lapse images of GFP::tubulin fluorescence, shown beginning during MI metaphase. Two phases of spindle shortening are observed. The initial phase is accompanied by an increase in microtubule density, consistent with an inward sliding mechanism, and ends at the time of spindle rotation (indicated by the arrow). The second phase begins 0.5 min after rotation and is accompanied by a decrease in mean microtubule density. Images of the spindle are shown above the corresponding time points, with the cortex outlined for clarity. Note the change in spindle shape during the second phase of shortening.

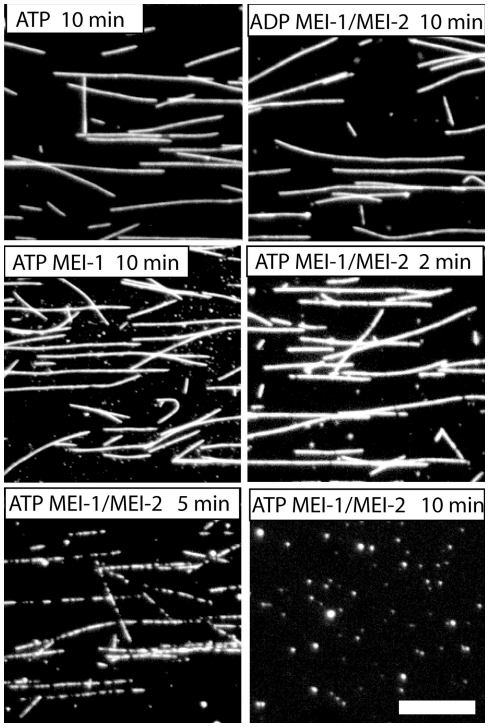

Figure 2. **The in vitro microtubule-severing activity of *C. elegans* MEI-1 is completely dependent on MEI-2.** Rhodamine-labeled, taxol-stabilized microtubules were immobilized on coverslip surfaces with a mutant kinesin at a final concentration of 0.1 μM tubulin dimer. Microtubules were perfused with solutions of ATP or ADP (1.8 mM) with MEI-1 alone or MEI-1–MEI-2 complexes (1.9 μM). After incubation for the specified time, microtubules were fixed and imaged. In the presence of MEI-1, MEI-2, and ATP, severed microtubules were clearly visible at 5 min, and complete disassembly of microtubules was observed at 10 min. No microtubule severing was observed with MEI-1 alone at concentrations up to 4.7 μM. Bar, 12 μm.

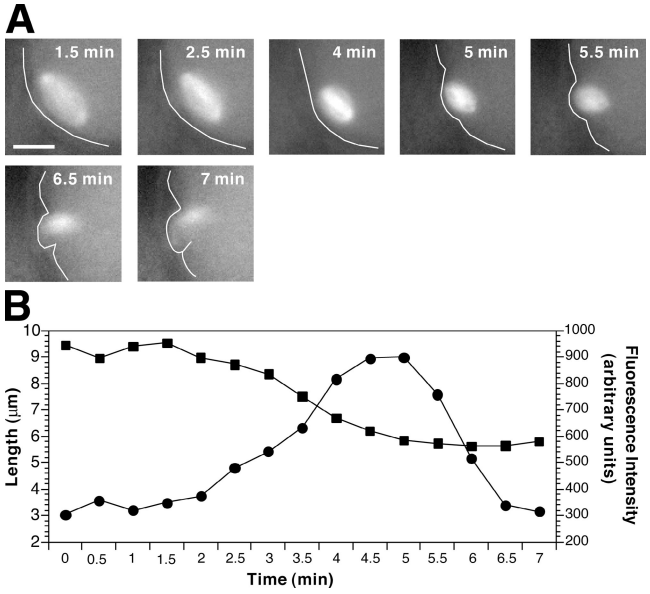

Figure 3. ***mei-2(ct98)* spindles shorten only by the early mechanism.** (A) Time-lapse images of an MI spindle in a *mei-2(ct98)* GFP::tubulin embryo were captured beginning at metaphase. This spindle shortened from 9.34 to 5.7 μm. It did not rotate until the cortex invaginated around it. Brightness has been adjusted for the later images to increase visibility of the spindle. The cortex has been outlined for clarity. Bar, 6 μm. (B) Graph of spindle length (squares) and fluorescence intensity (circles) beginning 2 min before the start of shortening. MT density initially increased and then decreased as in wild type; however, the spindle shortened only during the initial stage of increasing density.

MEI-1 for the first time (Fig. 2) and found that MEI-2 is absolutely required for the microtubule-severing activity of MEI-1. Thus, MEI-1 differs from katanin catalytic subunits from sea urchin (Hartman et al., 1998), human (McNally et al., 2000), or *Arabidopsis thaliana* (Stoppin-Mellet et al., 2002), each of which sever microtubules on their own. The MEI-2 dependence of MEI-1 suggests that *mei-2(ct98)* meiotic spindles should have a reduced amount of microtubule-severing activity. *mei-2(ct98)* worms were previously reported to lay viable embryos with large polar bodies (Mains et al., 1990), suggesting that these worms retain sufficient MEI-1–MEI-2 activity to assemble bipolar spindles but that these spindles might be unusually long at polar body induction.

Time-lapse imaging of a *mei-2(ct98)* strain expressing GFP::tubulin revealed that both the maximum and the minimum meiotic spindle lengths were considerably greater than in wild type (Table II). Wild-type spindles maintain a constant metaphase length before initiating shortening (Yang et al., 2003, 2005). If this steady-state length were the result of a balance between katanin-dependent shortening forces and katanin-independent lengthening forces, one might expect to see a period of spindle lengthening during metaphase in *mei-2(ct98)* embryos. Instead, *mei-2(ct98)* spindles maintained a constant length before initiating shortening in nine out of nine embryos that remained parallel to the plane of focus for 3 or more minutes during metaphase. This suggests that the increased maximum length of *mei-2(ct98)* spindles is a result of a defect during spindle assembly rather than a change in a balance of forces during metaphase.

The abnormally long metaphase spindles of *mei-2(ct98)* embryos shortened at a wild-type velocity of −0.95 μm/min to 6.2 μm for MI or 5.8 μm for MII during a period of increasing microtubule density but maintained a constant length as microtubule density decreased (Fig. 3 and Table II). The percentage of spindle shortening in *mei-2(ct98)* mutants (MI, 64%; MII, 63%) is similar to the percentage of shortening that is observed for wild-type spindles at the switch to decreasing microtubule density (MI, 58%; MII, 63%; see Table II), a transition that occurs nearly concurrently with spindle rotation. At this point, the velocity in *mei-2(ct98)* drops to −0.01 μm/min compared with −0.74 μm/min for wild type, and consequently the mutant spindle length remains at 65% of maximum, whereas that of wild type decreases to 38%. These results suggests that *mei-2(ct98)* spindles undergo the initial, sliding-dependent phase of shortening but do not undergo the second phase of shortening, which occurs after rotation in wild-type embryos. Consistent with this interpretation, chromosome separation in *mei-2(ct98)* spindles initiated within 1 min after spindle shortening ceased or microtubule density began decreasing ($n = 3$), just as separation initiated within 1 min after rotation in wild type ($n = 14$; McNally and McNally, 2005).

In contrast to wild-type spindles, which rotated at the time that microtubule density switches from increasing to decreasing,

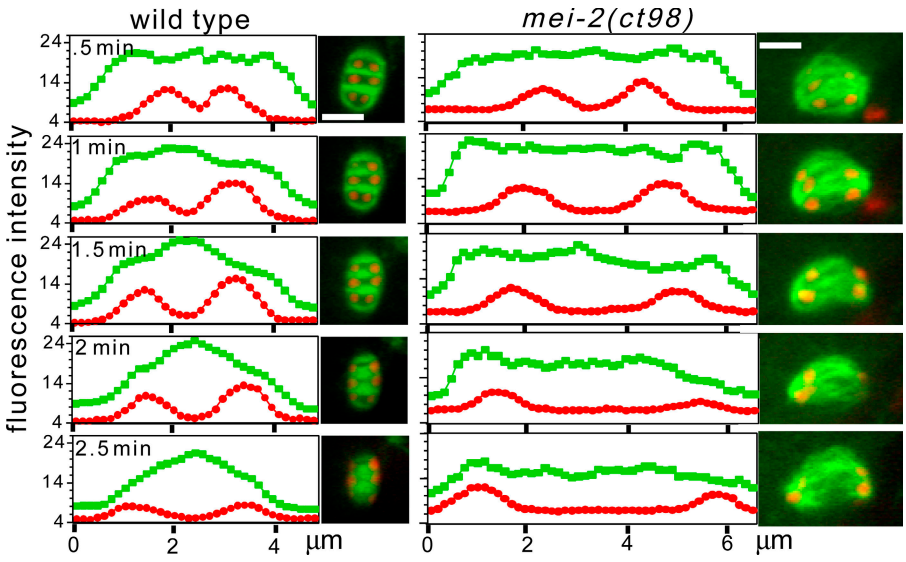

Figure 4. **The second phase of spindle shortening is accompanied by katanin-dependent redistribution of microtubules from the poles to the midzone.** Time-lapse images of a wild-type embryo and a *mei-2(ct98)* embryo expressing GFP::tubulin and mCherry::histone beginning at rotation were captured with a spinning-disk confocal microscope. Fluorescence intensity was plotted as a function of distance down the pole–pole axis of a single microtubule bundle for each image. Images are shown adjacent to their corresponding plots. Images are in the same orientation as the graphs. In the wild-type spindle, GFP::tubulin fluorescence intensity (green) of the spindle poles decreased, whereas the intensity of the spindle in between the separating chromosomes increased as the midzone formed. The *mei-2(ct98)* spindle, which did not shorten during this period, showed no change in the relative intensity of GFP::tubulin fluorescence at poles versus the midzone, but did exhibit a decrease in microtubule density that progressed uniformly throughout the spindle. Bars, 3.5 µm.

mei-2(ct98) spindles did not rotate (Fig. 3). The spindle remained parallel to the cortex as the cortex invaginated and, in the example shown in Fig. 3, only later turned toward the cell interior by the invagination of the cortex. The greatest angle at which *mei-2(ct98)* spindles interacted with the cortex was highly variable in contrast to wild-type spindles, which rotated to a near perfect 90° angle (Table II). Although it is possible that the MEI-2 gene product is directly required for spindle rotation, a second hypothesis is that rotation can only occur when the spindle has shortened to a critical length. Polar bodies in *mei-2(ct98)* embryos were larger and more variable in size than in wild-type embryos (Table II), suggesting that the wild-type function of spindle shortening and rotation is to minimize polar body size and thus preserve embryo volume.

The late phase of spindle shortening is mediated by katanin-dependent redistribution of microtubules

To more carefully compare changes in microtubule density during the late stage of spindle shortening, we used a strain expressing both GFP::tubulin and mCherry::histone to monitor spindle changes initiating at anaphase onset. Changes in the fluorescence intensity profiles down the pole–pole axis of a wild-type and a *mei-2(ct98)* spindle are shown in Fig. 4. In wild-type spindles, microtubule density in the spindle poles decreased, whereas microtubule density increased between the separating chromosomes. In contrast, *mei-2(ct98)* spindles exhibited a nearly uniform microtubule density down their pole–pole length and the relative density at the poles versus the midzone did not change over time. Similar results were obtained in 11 out of 11 wild-type embryos and 13 out of 13 *mei-2(ct98)* spindles. Thus, the microtubule-severing activity of MEI-1–MEI-2 katanin is required for the redistribution of microtubules from the spindle poles to the spindle midzone. Both wild-type (Fig. 1) and *mei-2(ct98)* spindles (Fig. 3) decrease in overall microtubule density after anaphase onset, indicating the additional action of katanin-independent microtubule depolymerizers in the reduction of overall microtubule density.

It could be that MEI-1–MEI-2 located at spindle poles is suddenly activated at anaphase onset, and its microtubule-severing activity promotes disassembly of spindle pole microtubules directly. It is also plausible that microtubule-severing activity

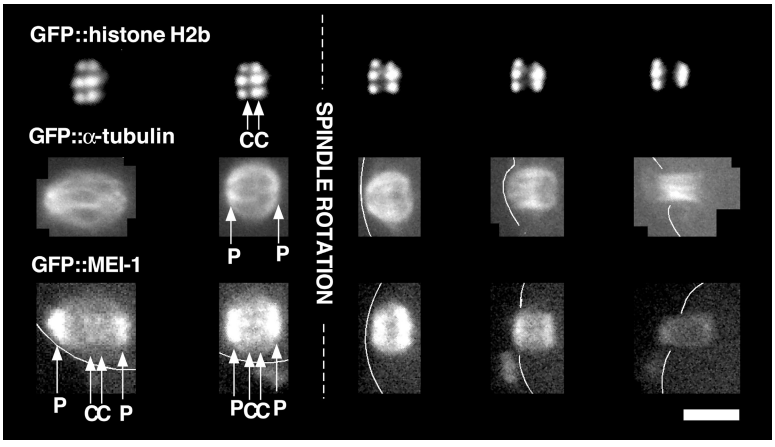

Figure 5. **Katanin localizes at spindle poles at the time of katanin-dependent microtubule redistribution.** Sequential time-lapse images of meiotic spindles in three different embryos expressing GFP::histone H2b, GFP::α-tubulin, or GFP::MEI-1. Each column contains images from spindles at an equivalent time point, and all images have been rotated so that the pole–pole axis runs from left to right. Arrows labeled C indicate chromosomes. In the metaphase configurations shown in the leftmost GFP::histone images, three out of six bivalents are in focus. Each horizontal pair of dots is one bivalent. Arrows labeled P indicate spindle poles. In the left pair of GFP::MEI-1 images, discrete signals at chromosomes and poles are visible. After spindle rotation and chromosome separation, chromosomes and poles are in almost the same positions. Bar, 6.5 µm.

during spindle assembly generates a wild-type spindle composed of overlapping short microtubules that are transported from the poles to the midzone after anaphase onset. In this case, *mei-2(ct98)* spindles would fail to undergo normal post-anaphase morphogenesis simply because they were composed of excessively long microtubules. To test when MEI-1–MEI-2 katanin might be acting, we examined the localization of GFP::MEI-1 by time-lapse imaging (Fig. 5 and Fig. S2, available at http://www.jcb.org/cgi/content/full/jcb.200608117/DC1). GFP::MEI-1 was localized uniformly on spindle microtubules during early stages of MI spindle assembly (not depicted) and subsequently concentrated on both spindle poles and on chromosomes (Fig. 5). The metaphase localization pattern was similar to that previously shown by immunofluorescence for both MEI-1 (Clark-Maguire and Mains, 1994a) and MEI-2 (Srayko et al., 2000). GFP::MEI-1 fluorescence intensity was the most intense and focused just after spindle rotation and when chromosomes had just reached the poles (Fig. 5). After this stage, GFP::MEI-1 fluorescence decreased substantially as the midbody lengthened (Fig. 5 and Fig. S2) and was then associated predominantly with chromosomes. The presence of GFP::MEI-1 at spindle poles just after rotation is consistent with a direct role of microtubule severing in the second phase of spindle shortening, and the decreasing intensity of GFP::MEI-1 at the end of this phase is consistent with the decreasing density of microtubules at spindle poles (Fig. 4).

The KLP-18 kinesin prevents meiotic spindle translocation in the absence of katanin

We previously reported that *mei-1(null)* spindles do not undergo timely translocation to the cortex (Yang et al., 2003). This translocation defect might indicate a direct role for microtubule severing in kinesin-dependent spindle translocation (Yang et al., 2005) or it might be an indirect consequence of the lack of antiparallel microtubule organization in *mei-1(null)* spindles. To test whether the spindle translocation defect in *mei-1(null)* mutants is simply a consequence of disorganized spindles, spindle translocation was examined in *klp-18(RNAi)* worms expressing either GFP::tubulin or GFP::histone. KLP-18 was chosen for this analysis because depletion of this motor was previously shown to have meiosis-specific spindle organization defects (Segbert et al., 2003). As shown in Table III, *klp-18(RNAi)* spindles, like wild-type spindles, translocated to the cortex either before the embryo exited the spermatheca or within 2 min of spermatheca exit. As previously reported (Yang et al., 2003), *mei-1(null)* spindles reached the cortex 9.9 ± 2.4 min after spermatheca exit. Surprisingly, this strong translocation defect in *mei-1(null)* mutants was completely suppressed by RNAi-mediated depletion of KLP-18 (Table III). These results indicate that (1) bipolar spindle organization is not required for timely spindle translocation, (2) the translocation defect in *mei-1(null)* mutants is a consequence of a KLP-18–dependent process, and (3) katanin is not directly required for spindle translocation. We suggest that in the absence of katanin, rigid, KLP-18–dependent microtubule bundles extend from the disorganized meiotic spindles and sterically inhibit movement toward the cortex.

Table III. **Timing of meiotic spindle translocation to the cortex**

Genotype	Spindles translocated while in the spermatheca	Spindles translocated after spermatheca exit	Time of translocation after spermatheca exit
			min
Wild type	8	4	1.3 ± 0.7 (n = 4)
mei-1(null)	0	19	9.9 ± 2.4 (n = 19)
klp-18 (RNAi)	7	2	0.5 ± 0.3 (n = 2)
mei-1(null) klp-18 (RNAi)	11	5	1.2 ± 0.6 (n = 5)

Katanin and γ-tubulin have redundant roles in meiotic spindle assembly

Although the spindle translocation defect in *mei-1(null)* mutants was suppressed by *klp-18(RNAi)*, bipolar spindles were still not assembled in *mei-1(null) klp-18(RNAi)* double mutants,

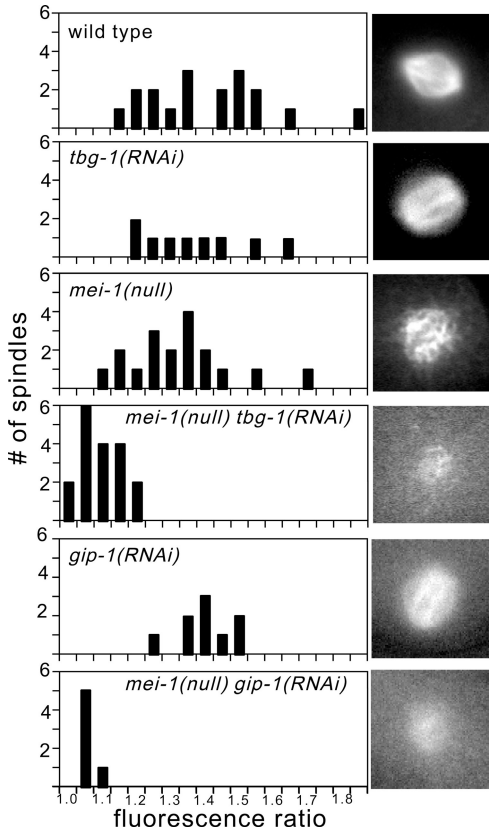

Figure 6. **γ-Tubulin and MEI-1 have redundant roles in microtubule assembly during meiotic spindle formation.** Images of MI metaphase spindles were captured in embryos expressing GFP::tubulin, and the mean microtubule density was expressed as the ratio of the mean pixel value of the spindle to the mean pixel value of the surrounding cytoplasm. Histograms indicate the number of spindles with the indicated fluorescence ratio for each genotype. The microtubule densities of spindles in embryos double depleted of both MEI-1 and either of the γ-TuRC subunits, TBG-1 or GIP-1, are markedly lower than those in embryos depleted of any protein alone. Representative images are shown next to each histogram. Brightness and contrast have been adjusted to allow visualization of spindle morphology.

indicating a direct role for katanin in spindle assembly. One possible role for katanin in spindle assembly was suggested by work on the plant cortical microtubule cytoskeleton, where katanin is required for formation of organized parallel/antiparallel microtubule bundles (Burk et al., 2001), just as it is in *C. elegans* meiosis. Plant cortical microtubules are nucleated from microtubule-associated γ-tubulin complexes at a discrete 42° angle from preexisting microtubules (Murata et al., 2005). It is intriguing to speculate that katanin-mediated severing might be required to release microtubules from these branched networks to allow parallel bundling. If this were the case with acentrosomal *C. elegans* meiotic spindles, then γ-tubulin (RNAi) might partially suppress the need for katanin in spindle assembly. An alternative hypothesis is based on the fact that microtubule severing and microtubule nucleation both have the same net effect of increasing microtubule number. In this hypothesis, katanin and γ-tubulin might have partially overlapping roles in increasing microtubule number early in spindle assembly. In this case, γ-tubulin (RNAi) would be expected to worsen the phenotype of a *mei-1(null)* mutant.

To test these hypotheses, GFP::tubulin-expressing worms were fed bacteria expressing *tbg-1* (γ-tubulin) or *gip-1* (γ-tubulin ring complex [γ-TuRC] subunit) double-stranded RNA for 40–44 h. This amount of time is required to deplete maternal protein from the syncytial gonad. Longer feeding regimens resulted in oogenesis defects and failures in ovulation. Meiotic spindle morphology appeared wild type in *tbg-1(RNAi)* or *gip-1(RNAi)* worms (Fig. 6), consistent with previous reports of normal polar body size and number (Strome et al., 2001). Microtubule density, as determined from the ratio of mean GFP::tubulin fluorescence in the spindle to fluorescence in the cytoplasm, was similar between wild-type, *mei- 1(null)*, *tbg-1(RNAi)*, and *gip-1(RNAi)* spindles but was dramatically reduced in *mei-1(null)*; *tbg-1(RNAi)* or *mei-1(null)*; *gip-1(RNAi)* double-mutant spindles (Fig. 6). This synthetic effect was not observed in *mei-1(null)*; *klp-18(soaking RNAi)* double-mutant worms (Fig. S3, available at http://www.jcb.org/cgi/cotnent/full/jcb.200608117/DC1), indicating that the enhancement was specific. Neither *tbg-1(RNAi)* nor *gip-1(RNAi)* suppressed the spindle morphology defect in *mei-1(null)* worms. Because *tbg-1(RNAi)* and *gip-1(RNAi)* enhanced rather than suppressed the spindle morphology defect in *mei-1(null)* worms, these results suggest that MEI-1 and γ-tubulin play redundant roles rather than antagonistic roles in promoting increasing microtubule density during spindle assembly. In addition, because the *mei-1(null)* mutant completely lacks function, we can conclude that MEI-1 and γ-tubulin are acting in parallel rather than sequentially.

If this hypothesis were correct, then MEI-1 and γ-tubulin should both be present at the time and place that meiotic spindle assembly initiates. As shown in Fig. 7 A, meiotic spindle assembly initiates at nuclear envelope breakdown, when a diffuse cloud of microtubules fills the volume of the perforated nucleus. These microtubules then organize into a much smaller assembly of dense microtubule bundles by the time the oocyte ovulates into the spermatheca (Fig. 7 A; Yang et al., 2003). By the time the embryo exits the spermatheca and enters the uterus, a bipolar, metaphase-length spindle is present within a vesicle-free zone visible by differential interference contrast (Fig. 7 C). Before NEBD, GFP::TBG-1 became progressively more concentrated on the nuclear envelope as oocyte maturation progressed (Fig. 7 B). At nuclear envelope breakdown, GFP::TBG-1 fluorescence entered the nuclear region, forming a diffuse cloud that might indicate association with either microtubules or vesicles derived from the nuclear envelope. This large, diffuse area of γ-tubulin enrichment did not contract in diameter nor increase in local intensity (Fig. 7 B), as did the α-tubulin (Fig. 7 A). By the time the embryo exited the spermatheca into the uterus, no discrete localization of GFP::TBG-1 was observed in the

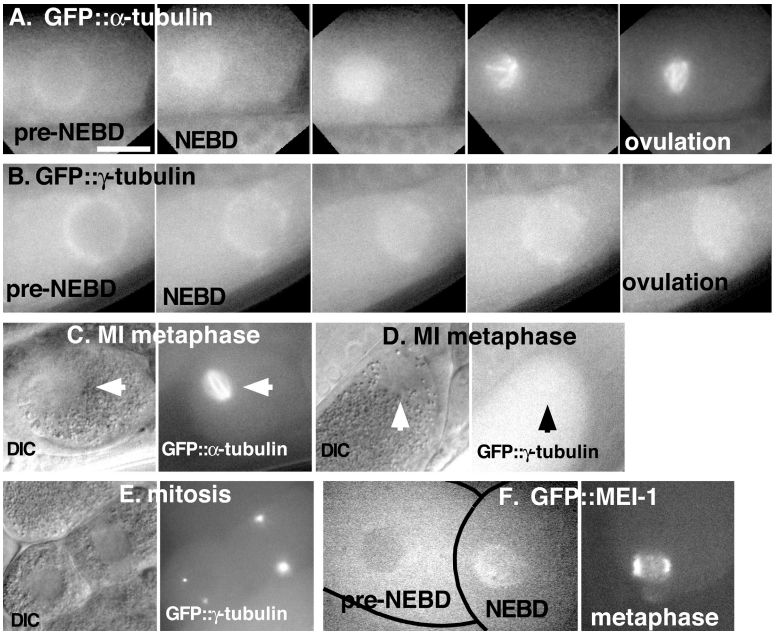

Figure 7. **MEI-1 and γ-tubulin enter the nucleus at the time that meiotic spindle assembly is initiated.** (A) Time-lapse images of a maturing oocyte expressing GFP::α-tubulin show that, before nuclear envelope breakdown (NEBD), tubulin is excluded from the nucleus. During NEBD, tubulin entered the nuclear region. After NEBD, a cloud of increased fluorescence filled the volume of the perforated nucleus. We interpret this cloud of increased fluorescence as a cloud of microtubules filling the volume of the perforated nucleus. This cloud of microtubules then contracted and organized into a group of thick bundles by ovulation. (B) Time-lapse images of a maturing oocyte expressing GFP::γ-tubulin show that γ-tubulin is concentrated around the nuclear envelope before NEBD and then localizes to a diffuse cloud filling the volume of the perforated nucleus until ovulation. (C) Embryos that have just moved from the spermatheca to the uterus exhibit a vesicle-free zone in differential interference contrast (DIC) that contains the metaphase I spindle. (D) No discrete localization of GFP::γ-tubulin could be discerned within the vesicle-free zone at this time point, although diffuse cytoplasmic fluorescence was visible and GFP::γ-tubulin clearly labeled mitotic centrosomes (E) after the completion of meiosis. (F) Images of GFP::MEI-1 fluorescence showing an oocyte before NEBD (left) and maturing oocyte just after NEBD (right). Before NEBD, GFP::MEI-1 is distributed throughout the cytoplasm and is excluded from the nucleus. After NEBD occurs, the protein first localizes to a diffuse cloud and then becomes concentrated at poles and chromosomes as the spindle assembles. Bar, 12 μm.

vesicle-free zone that contains the metaphase I spindle (Fig. 7 D). GFP::MEI-1 was also distributed throughout the volume of the perforated nucleus immediately after nuclear envelope breakdown (Fig. 7 F). GFP::MEI-1 differed from GFP::TBG-1 in that it became highly concentrated on chromosomes and spindle poles during spindle assembly and remained concentrated on these structures throughout meiosis (Fig. 7 F, Fig. 5, and Fig. S2). The transient presence of microtubules, MEI-1, and γ-tubulin within the perforated nucleus immediately after nuclear envelope breakdown is consistent with the hypothesis that microtubule severing and γ-TuRC–templated nucleation provide redundant mechanisms for increasing microtubule number during the initial stages of spindle assembly.

Discussion

Katanin and spindle length

Our results demonstrate that inhibition of katanin inhibits spindle-shortening processes in fibroblast mitotic spindles and *C. elegans* meiotic spindles. Mitotic spindles of cultured mammalian cells do not normally shorten, but intrinsic shortening processes can be revealed when microtubule polymerization is blocked with nocodazole or taxol (Cassimeris and Salmon, 1991; Waters et al., 1996; Mitchison et al., 2005). These shortening processes are opposed by kinesin-5–dependent outward sliding forces (Brust-Mascher and Scholey, 2002), which depend on bundles of overlapping microtubules. We propose that untreated CV1 spindles are composed of discontinuous arrays of overlapping microtubules generated by a combination of microtubule severing near the poles and dynamic instability (Fig. 8 A; Buster et al., 2002). Short microtubules result in short overlap regions, which are lost rapidly during nocodazole treatment. The rapid loss of outward sliding forces allows rapid spindle shortening, which is possibly due to the inward squeezing "tensile element" (Mitchison et al., 2005). In this scenario, spindles are composed of more contiguous long microtubules after katanin inhibition, and these longer microtubules have long overlap zones that oppose spindle shortening forces for a longer time period during nocodazole treatment (Fig. 8 B).

C. elegans female meiotic spindles naturally undergo dramatic shortening cycles during each anaphase. Our results indicate that this shortening is initially driven by katanin-independent spindle shortening that is accompanied by increasing microtubule density and may be driven by inward sliding of antiparallel microtubules (Fig. 8 C). This phase is followed by a katanin-dependent phase in which microtubule density decreases at poles and increases in the midzone. We favor a model for late shortening in which katanin, localized at spindle poles, severs pole-proximal microtubules into short fragments that are then transported to the midzone (Fig. 8 E). The second phase of spindle shortening is also accompanied by a katanin-independent decrease in the overall density of spindle microtubules that may be caused by other microtubule-destabilizing proteins.

Katanin and spindle assembly

The increased steady-state metaphase spindle length in the partial-loss-of-function katanin mutant is consistent with a model in which wild-type meiotic spindles are assembled as an array of discontinuous, overlapping, short microtubules (Fig. 8 C), just as we propose for CV1 mitotic spindles (Fig. 8 A). A reduced rate of microtubule severing results in a longer spindle because mean microtubule length is longer. This increased microtubule length would limit the extent of spindle shortening by the early, inward sliding mechanism (Fig. 8, C and D; and

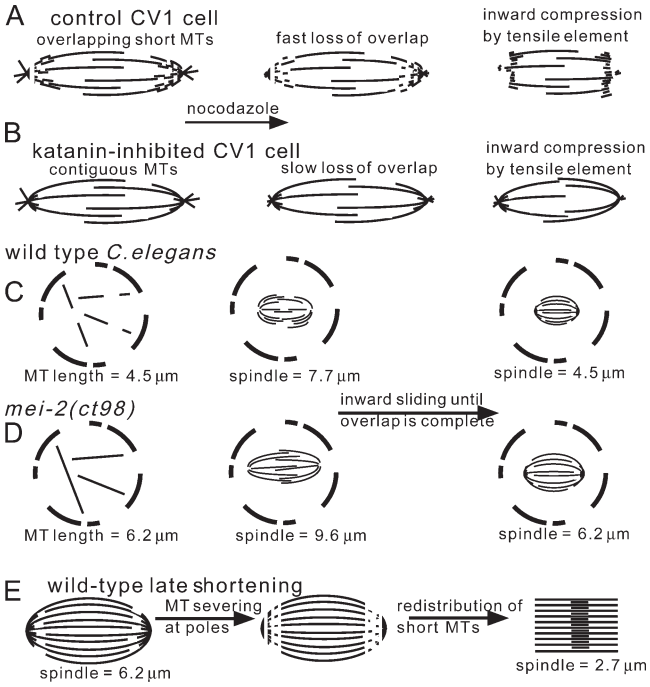

Figure 8. **Detailed model for the action of katanin during CV1 cell mitosis and *C. elegans* meiosis.** (A) We propose that CV1 cell mitotic spindle poles consist of short, overlapping microtubule arrays generated by katanin-mediated microtubule severing at poles and cross-bridged by the combined actions of cytoplasmic dynein and Eg5. Nocodazole-mediated microtubule depolymerization results in a rapid loss of microtubule overlap that is required for dynein and Eg5 to maintain spindle structure. In the absence of cross-bridged overlap, there would be no resistance to inward contraction by a tensile element or to inward force generated by plus-end depolymerization at kinetochores. (B) Mitotic spindles in katanin-inhibited CV1 cells are composed of longer, more contiguous microtubule arrays. More time is thus required for nocodazole to cause a loss of microtubule overlap and, therefore, a loss of resistance to inward forces. (C) During wild-type *C. elegans* germinal vesicle breakdown, microtubules with a mean length of 4.5 μm assemble because of the combined effects of dynamic instability and katanin-dependent microtubule severing. These microtubules assemble into a 7.7-μm-long metaphase spindle composed of overlapping microtubules. During the first phase of spindle shortening, microtubules slide inward until they completely overlap, generating a 4.5-μm-long spindle that has twice the microtubule density as the metaphase spindle. (D) In *mei-2(ct98)* oocytes, microtubules assemble at germinal vesicle breakdown with a mean length of 6.2 μm because of the absence of microtubule severing. These microtubules assemble into a 9.6-μm-long metaphase spindle that shortens by inward sliding until the 6.2-μm microtubules completely overlap, resulting in a 6.2-μm-long spindle that does not shorten further. (E) After completion of inward sliding, 4.5-μm-long wild-type meiotic spindles undergo a transition that is marked by spindle rotation, initiation of chromosome separation, and a switch from increasing to decreasing microtubule density. MEI-1 is concentrated at spindle poles at this time, and we suggest that severing of microtubules at the poles allows a redistribution of short microtubules from the poles to the midzone. The redistribution of microtubule density and the further shortening to 2.7 μm that occur in wild type do not occur in *mei-2(ct98)* embryos because of a lack of microtubule severing at spindle poles.

Table II). Our model is qualitatively consistent with the EM tomography results of Srayko et al. (2006), who found many short microtubules in a wild-type spindle but only long microtubules in a *mei-1(null)* spindle. It is more difficult to resolve our model quantitatively with the EM tomography data, however, because more than half the microtubules in this tomogram extended beyond the tomogram and thus could not be measured.

The finding of numerous short microtubules in a wild-type meiotic spindle and the lack of short microtubules in a *mei-1(null)* spindle (Srayko et al., 2006) is also qualitatively consistent with our finding that katanin and γ-TuRC have partially redundant roles in promoting microtubule density increase during spindle assembly. Our results with GFP-tubulin fluorescence intensity measurements revealed microtubule densities that were similar between wild-type metaphase spindles and *mei-1(null)* spindles (Fig. 6). We propose that this difference is small because γ-TuRC–mediated nucleation can increase microtubule number in the absence of severing activity. This result is consistent with the small (25%) difference in polymer mass determined from fixed immunofluorescence analysis by Srayko et al. (2006).

Perhaps the most perplexing question remaining is why *mei-1(null)* mutants do not assemble extremely long bipolar spindles similar to what is seen with the partial-loss-of-function *mei-2* mutant. We offer two hypotheses explaining the absolute requirement for katanin in *C. elegans* meiotic spindle assembly. In the first hypothesis, MEI-1–MEI-2 complexes have an additional, nonsevering function, such as cross-bridging antiparallel microtubules or recruiting other essential proteins to the spindle. In this scenario, *mei-2(ct98)* spindles actually have no microtubule-severing activity but can assemble bipolar spindles with a low concentration of MEI-1–MEI-2 cross-bridging activity. This cross-bridging activity may be more critical in noncentrosomal microtubule arrays. The nonlinear dependence of microtubule-severing activity on katanin concentration (Hartman and Vale, 1999) supports the notion that a reduced amount of MEI-2 could result in a complete loss of severing activity. In the second hypothesis, mean microtubule length increases as katanin concentration decreases until a critical stage is reached where microtubules are too long to allow spindle assembly. In the *C. elegans* meiotic embryo, the relative activities of other critical regulators of microtubule dynamics and motility would be optimized for assembling spindles from short microtubules. These other microtubule-binding proteins would then assemble aberrant structures from long microtubules.

The conserved localization of katanin at spindle poles of many species and the similarity of spindle-length phenotypes in CV1 cells and *C. elegans* meiotic spindles suggests that katanin regulates mitotic and meiotic spindle length in many species. The generality of katanin's relative role in the assembly of mitotic versus meiotic spindles remains to be elucidated. Our dominant-negative inhibitors did not prevent mitotic spindle assembly in CV1 cells (Buster et al., 2002); however, genome sequences reveal that human and mouse each have three distinct katanin catalytic subunits (unpublished data) as well as the related microtubule-severing ATPase, spastin. These different microtubule-severing proteins could easily have unique roles at different times in development.

Materials and methods

Transfection of CV1 cells

CV1 cells with an integrated YFP-tubulin construct were transfected on 25-mm coverslips with Lipofectamine Plus (Invitrogen) using CFP-X plasmid constructs, which were described previously (Buster et al., 2002). 12–20 h after transfection, coverslips were assembled into perfusion chambers maintained at 37°C. Cells were imaged with a microscope (Microphot SA; Nikon) equipped with a 60× Plan Apo 1.4 objective, a charge-coupled device (CCD; Quantix KAF1400; Photometrics), and Ludl shutter controlled by IP Lab Spectrum software. Mitotic CFP-expressing cells were identified quickly using reduced illumination. A single CFP fluorescence image was captured using fixed neutral density filters, exposure, and gain so that the expression level could be estimated. 50 μl of culture medium containing 80 μM nocodazole was then added gently to the edge of the perfusion chamber and shuttered, and time-lapse acquisition of YFP fluorescence images was initiated. Diffusion of nocodazole to the imaged cell did not appear to be rate limiting, as the fastest changes in spindle length always occurred in the first 5 s of the image sequence.

Microtubule-severing assays

A cDNA encoding the long isoform of MEI-1 (Clark-Maguire and Mains, 1994b) was cloned as a 6-his–tagged fusion along with an untagged MEI-2 cDNA into pFastBac Dual (Invitrogen), expressed in Sf9 cells using the Bac to Bac System (Invitrogen) and partially purified by Ni^{2+}-chelate chromatography.

A 1:10 mixture of tetra-methy-rhodamine–labeled and unlabeled porcine brain tubulin was polymerized and stabilized with 20 μM taxol. Microtubules were immobilized on the surfaces of perfusion chambers at a final concentration of 0.1 μM tubulin dimer using an *Escherichia coli*–expressed G234A mutant of the first 560 amino acids of ubiquitous human kinesin heavy chain. Preparations of purified MEI-1 or MEI-1–MEI-2 complexes were perfused at final concentrations ranging from 0.5 to 5.7 μM in 20 mM K-Hepes, pH 7.5, 0.1 mM EGTA, and 2 mM $MgSO_4$ with ATP or ADP at 1.8 mM. Reactions were stopped at time intervals by perfusion with glutaraldehyde, and images of fixed microtubules were captured with a CCD.

C. elegans strains

In this study, wild type indicates one of several integrated transgenic strains. The integrated GFP::tubulin strain WH204 (Strome et al., 2001) was used for the studies shown in Figs. 1 and 3 and Tables II and III. The integrated GFP::tubulin strain AZ244 (Praitis et al., 2001) was consistently brighter than WH204 and was used for the studies shown in Figs. 5, 6, and 7. The integrated GFP::histone H2b strain AZ212 (Praitis et al., 2001) was used in Fig. 5. The integrated GFP::tubulin, mCherry::histone strain, OD57, was the wild type used for Fig. 4. OD57 was generated by particle bombardment of a *pie-1* promoter vector (Praitis et al., 2001) engineered to express a histone H2b fusion to a version of mCherry (Shaner et al., 2004) that included four *C. elegans* introns and *C. elegans* preferred codons. This modified mCherry DNA was synthesized by Molecular Cloning Laboratories. The mCherry::histone strain was crossed with the GFP::tubulin-expressing strain, OD4, to obtain OD57. *mei-2(ct98)* worms were obtained from P. Mains (University of Calgary, Calgary, Canada) and were crossed with WH204 to obtain *mei-2(ct98)* worms expressing GFP::tubulin, with AZ212 to obtain *mei-2(ct98)* worms expressing GFP::histone H2b and with OD57 to obtain *mei-2(ct98)* worms expressing both GFP::tubulin and mCherry::histone. The *mei-1(null)* allele used in this study was the nonsense mutant *mei-1(ct46ct101)* (Clark-Maguire and Mains, 1994b). Homozygous *mei-1(ct46ct101)* worms expressing GFP::tubulin and used for the studies shown in Table III were described previously (Yang et al., 2003). For data shown in Fig. 6, homozygous *mei-1(ct46ct101)* worms expressing a higher level of GFP::tubulin were derived from crosses between HR1069 (*unc-13[e10910] daf-8[e1393] mei-1[ct46ct101]*/hT2*[bli-4{e937} let{h661]}* I; hT2/+ III] and AZ244. The GFP::MEI-1-expressing strain was EU1065 (Pintard et al., 2003). Western blots with anti–MEI-1 antibody indicated that this transgene is expressed at a much lower level than endogenous MEI-1 (not depicted), indicating that the localization in Fig. 5 is not due to overexpression. OD44, the GFP::γ tubulin-expressing strain used in Fig. 7, was provided by A. Desai (University of California, San Diego, La Jolla, CA). *mei-2(ct98)* strains were maintained at 16°C and shifted

to 20°C for 24 h before filming. EU1065 was maintained at 25°C to prevent germline silencing. All other strains were maintained at 20°C.

In utero filming of meiotic spindles

Adult hermaphrodites were anesthetized with Tricaine/tetramisole as described previously (Kirby et al., 1990; McCarter et al., 1999) and gently mounted between a coverslip and a thin agarose pad on a slide. Mineral oil or petroleum jelly was used to reduce evaporation at the edge of the coverslip. Images for Figs. 1, 2, and 3; histograms in Fig. 6; most of Fig. 7; and data for all tables were acquired on a microscope (Microphot SA; Nikon) as described for CV1 cell imaging. Images in Figs. 4 and 5, parts of Fig. 6, and Fig. S2 were acquired with a spinning-disk confocal microscope (Perkin-Elmer) equipped with an 100× Plan Apo 1.35 objective (Olympus), CCD (Orca ER; Hamamatsu), and Slidebook acquisition software. All quantitative analysis was performed with IP Lab Spectrum software (Scanalytics).

Analysis of spindle length and microtubule density

Spindle length in individual time-lapse images was determined using the Measure Length function of IP Lab Spectrum. The majority of spindle-length measurements were made from single focal plane, wide field images. Only spindles parallel to the plane of focus were used for this analysis. Either of two criteria was used to determine that a spindle was parallel to the plane of focus rather than rotating into the plane of focus to give the impression of shortening. First, the shape of both spindle poles appears identical only when the spindle is parallel to the plane of focus. Second, bundles of microtubules extending all the way between spindle poles are observed only when the spindle is parallel to the plane of focus. Note that the primary result of this paper is a lack of a late phase of spindle shortening that cannot be explained by any optical artifact.

Mean microtubule density in the entire spindle as shown in Figs. 1, 3, and 6 was determined in IP Lab Spectrum by highlighting the entire spindle as a "segment" and determining the mean pixel value within the entire segment. This measurement is proportional to microtubule density as opposed to microtubule mass, which would be proportional to the sum of the values of all of the pixels within a spindle. Three separate segments that encompassed most of one spindle pole, most of the middle quarter of the spindle, and a band between the spindle pole and the middle quarter of the spindle were used to repeat this analysis. During the period of overall density increase shown in Figs. 1 and 3, density (mean pixel value) increased uniformly in these three segments (not depicted). After spindle rotation, mean pixel values in these three segments behaved differently (not depicted), so line scan analysis (Fig. 4) was used to illustrate these more complex intensity changes.

Line scans of fluorescence intensity shown in Fig. 4 were generated in the following manner. GFP::tubulin labeled discrete bundles of microtubules running from pole to pole. Exactly four of these bundles are visible in the wild-type spindle shown in Fig. 4. The ROI (region of interest) line tool in IP Lab Spectrum was used to draw a line down the length of one of these bundles. For wild type, a straight line was used. For *mei-2(ct98)*, an irregular line was drawn to follow one of the irregular microtubule bundles. The ROI boundary function of IP Lab was then used to determine the pixel value at each point along this line, and these values were plotted as a function of spindle length in DeltaGraph. mCherry-histone–labeled chromosomes were between the microtubule bundles. Thus, a second line was drawn from pole to pole that passed over one chromosome pair to plot the anaphase movement of one chromosome pair.

RNAi

Depletion of KLP-18 was accomplished by soaking worms in double-stranded RNA produced from cDNA clone yk745f12 provided by Y. Kohara (National Institute of Genetics, Mishima, Japan) using previously described methods (Yang et al., 2005). γ-TuRC subunits were depleted by RNAi by feeding using clones III-5K19 (*tbg-1*) and III-1F05 (*gip-1*) (MRC Gene Services; Kamath et al., 2003).

Online supplemental material

Fig. S1 shows purification of recombinant MEI-1–MEI-2. Fig. S2 shows that katanin localizes at spindle poles at the time of katanin-dependent microtubule redistribution. Fig. S3 shows that *mei-1(null); klp-18(RNAi)* double mutants do not show the synthetic effect on microtubule density observed in *mei-1(null); tbg-1(RNAi)* double mutants. Online supplemental material is available at http://www.jcb.org/cgi/content/full/jcb.200608117/DC1.

We thank the *C. elegans* Genetics Center, Paul Mains, Bruce Bowerman, Arshad Desai, and John White for strains; Yuji Kohara for cDNA clones; Roger Tsien for mCherry; and Jon Scholey and Ingrid Brust-Mascher for assistance with spinning-disk confocal microscopy. We also thank Lesilee Rose and Dan Starr for critical discussions and facilities.

This work was supported by a grant from the University of California Cancer Research Coordinating Committee.

Submitted: 21 August 2006
Accepted: 20 November 2006

References

Bishop, J.D., Z. Han, and J.M. Schumacher. 2005. The *Caenorhabditis elegans* Aurora B kinase AIR-2 phosphorylates and is required for the localization of a BimC kinesin to meiotic and mitotic spindles. *Mol. Biol. Cell.* 16:742–756.

Brust-Mascher, I., and J.M. Scholey. 2002. Microtubule flux and sliding in mitotic spindles of *Drosophila* embryos. *Mol. Biol. Cell.* 13:3967–3975.

Burk, D.H., B. Liu, R. Zhong, W.H. Morrison, and Z.H. Ye. 2001. A katanin-like protein regulates normal cell wall biosynthesis and cell elongation. *Plant Cell.* 13:807–827.

Buster, D., K. McNally, and F.J. McNally. 2002. Katanin inhibition prevents the redistribution of gamma-tubulin at mitosis. *J. Cell Sci.* 115:1083–1092.

Cassimeris, L., and E.D. Salmon. 1991. Kinetochore microtubules shorten by loss of subunits at the kinetochores of prometaphase chromosomes. *J. Cell Sci.* 98:151–158.

Clark-Maguire, S., and P.E. Mains. 1994a. Localization of the *mei-1* gene product of *Caenorhabditis elegans*, a meiotic-specific spindle component. *J. Cell Biol.* 126:199–209.

Clark-Maguire, S., and P.E. Mains. 1994b. *mei-1*, a gene required for meiotic spindle formation in *Caenorhabditis elegans*, is a member of a family of ATPases. *Genetics.* 136:533–546.

Gandhi, R., S. Bonaccorsi, D. Wentworth, S. Doxsey, M. Gatti, and A. Pereira. 2004. The *Drosophila* kinesin-like protein KLP67A is essential for mitotic and male meiotic spindle assembly. *Mol. Biol. Cell.* 15:121–131.

Ganem, N.J., K. Upton, and D.A. Compton. 2005. Efficient mitosis in human cells lacking poleward microtubule flux. *Curr. Biol.* 15:1827–1832.

Goshima, G., R. Wollman, N. Stuurman, J.M. Scholey, and R.D. Vale. 2005. Length control of the metaphase spindle. *Curr. Biol.* 15:1979–1988.

Grill, S.W., P. Gonczy, E.H. Stelzer, and A.A. Hyman. 2001. Polarity controls forces governing asymmetric spindle positioning in the *Caenorhabditis elegans* embryo. *Nature.* 409:630–633.

Hartman, J.J., and R.D. Vale. 1999. Microtubule disassembly by ATP-dependent oligomerization of the AAA enzyme katanin. *Science.* 286:782–785.

Hartman, J.J., J. Mahr, K. McNally, K. Okawa, A. Iwamatsu, S. Thomas, S. Cheesman, J. Heuser, R.D. Vale, and F.J. McNally. 1998. Katanin, a microtubule-severing protein, is a novel AAA ATPase that targets to the centrosome using a WD40-containing subunit. *Cell.* 93:277–287.

Hoyt, M.A., L. He, K.K. Loo, and W.S. Saunders. 1992. Two *Saccharomyces cerevisiae* kinesin-related gene products required for mitotic spindle assembly. *J. Cell Biol.* 118:109–120.

Kamath, R.S., A.G. Fraser, Y. Dong, G. Poulin, R. Durbin, M. Gotta, A. Kanapin, N. Le Bot, S. Moreno, M. Sohrmann, et al. 2003. Systematic functional analysis of the *Caenorhabditis elegans* genome using RNAi. *Nature.* 421:231–237.

Kapitein, L.C., E.J. Peterman, B.H. Kwok, J.H. Kim, T.M. Kapoor, and C.F. Schmidt. 2005. The bipolar mitotic kinesin Eg5 moves on both microtubules that it crosslinks. *Nature.* 435:114–118.

Kirby, C., M. Kusch, and K. Kemphues. 1990. Mutations in the *par* genes of *Caenorhabditis elegans* affect cytoplasmic reorganization during the first cell cycle. *Dev. Biol.* 142:203–215.

Maddox, P.S., K.S. Bloom, and E.D. Salmon. 2000. The polarity and dynamics of microtubule assembly in the budding yeast *Saccharomyces cerevisiae*. *Nat. Cell Biol.* 2:36–41.

Maiato, H., A. Khodjakov, and C.L. Rieder. 2005. *Drosophila* CLASP is required for the incorporation of microtubule subunits into fluxing kinetochore fibers. *Nat. Cell Biol.* 7:42–47.

Mains, P.E., K.J. Kemphues, S.A. Sprunger, I.A. Sulston, and W.B. Wood. 1990. Mutations affecting the meiotic and mitotic divisions of the early *Caenorhabditis elegans* embryo. *Genetics.* 126:593–605.

Mallavarapu, A., K. Sawin, and T. Mitchison. 1999. A switch in microtubule dynamics at the onset of anaphase B in the mitotic spindle of *Schizosaccharomyces pombe*. *Curr. Biol.* 9:1423–1426.

McCarter, J., B. Bartlett, T. Dang, and T. Schedl. 1999. On the control of oocyte meiotic maturation and ovulation in *Caenorhabditis elegans*. *Dev. Biol.* 205:111–128.

McNally, F.J., and S. Thomas. 1998. Katanin is responsible for the M-phase microtubule-severing activity in *Xenopus* eggs. *Mol. Biol. Cell.* 9:1847–1861.

McNally, F.J., K. Okawa, A. Iwamatsu, and R.D. Vale. 1996. Katanin, the microtubule-severing ATPase, is concentrated at centrosomes. *J. Cell Sci.* 109:561–567.

McNally, K.L., and F.J. McNally. 2005. Fertilization initiates the transition from anaphase I to metaphase II during C. elegans meiosis. *Dev. Biol.* 282: 218–230.

McNally, K.P., O.A. Bazirgan, and F.J. McNally. 2000. Two domains of p80 katanin regulate microtubule severing and spindle pole targeting by p60 katanin. *J. Cell Sci.* 113:1623–1633.

Mitchison, T.J. 1989. Polewards microtubule flux in the mitotic spindle: evidence from photoactivation of fluorescence. *J. Cell Biol.* 109:637–652.

Mitchison, T.J., P. Maddox, J. Gaetz, A. Groen, M. Shirasu, A. Desai, E.D. Salmon, and T.M. Kapoor. 2005. Roles of polymerization dynamics, opposed motors, and a tensile element in governing the length of *Xenopus* extract meiotic spindles. *Mol. Biol. Cell.* 16:3064–3076.

Mountain, V., C. Simerly, L. Howard, A. Ando, G. Schatten, and D.A. Compton. 1999. The kinesin-related protein, HSET, opposes the activity of Eg5 and cross-links microtubules in the mammalian mitotic spindle. *J. Cell Biol.* 147:351–366.

Murata, T., S. Sonobe, T.I. Baskin, S. Hyodo, S. Hasezawa, T. Nagata, T. Horio, and M. Hasebe. 2005. Microtubule-dependent microtubule nucleation based on recruitment of gamma-tubulin in higher plants. *Nat. Cell Biol.* 7:961–968.

Pintard, L., T. Kurz, S. Glaser, J.H. Willis, M. Peter, and B. Bowerman. 2003. Neddylation and deneddylation of CUL-3 is required to target MEI-1/Katanin for degradation at the meiosis-to-mitosis transition in *C. elegans*. *Curr. Biol.* 13:911–921.

Praitis, V., E. Casey, D. Collar, and J. Austin. 2001. Creation of low-copy integrated transgenic lines in *Caenorhabditis elegans*. *Genetics.* 157:1217–1226.

Rogers, G.C., S.L. Rogers, T.A. Schwimmer, S.C. Ems-McClung, C.E. Walczak, R.D. Vale, J.M. Scholey, and D.J. Sharp. 2004. Two mitotic kinesins cooperate to drive sister chromatid separation during anaphase. *Nature.* 427:364–370.

Segbert, C., R. Barkus, J. Powers, S. Strome, W.M. Saxton, and O. Bossinger. 2003. KLP-18, a Klp2 kinesin, is required for assembly of acentrosomal meiotic spindles in *Caenorhabditis elegans*. *Mol. Biol. Cell.* 14:4458–4469.

Shaner, N.C., R.E. Campbell, P.A. Steinbach, B.N. Giepmans, A.E. Palmer, and R.Y. Tsien. 2004. Improved monomeric red, orange and yellow fluorescent proteins derived from *Discosoma* sp. red fluorescent protein. *Nat. Biotechnol.* 22:1567–1572.

Sharp, D.J., K.R. Yu, J.C. Sisson, W. Sullivan, and J.M. Scholey. 1999. Antagonistic microtubule-sliding motors position mitotic centrosomes in *Drosophila* early embryos. *Nat. Cell Biol.* 1:51–54.

Srayko, M., D.W. Buster, O.A. Bazirgan, F.J. McNally, and P.E. Mains. 2000. MEI-1/MEI-2 katanin-like microtubule severing activity is required for *Caenorhabditis elegans* meiosis. *Genes Dev.* 14:1072–1084.

Srayko, M., E.T. O'Toole, A.A. Hyman, and T. Muller-Reichert. 2006. Katanin disrupts the microtubule lattice and increases polymer number in *C. elegans* meiosis. *Curr. Biol.* 16:1944–1949.

Stoppin-Mellet, V., J. Gaillard, and M. Vantard. 2002. Functional evidence for in vitro microtubule severing by the plant katanin homologue. *Biochem. J.* 365:337–342.

Strome, S., J. Powers, M. Dunn, K. Reese, C.J. Malone, J. White, G. Seydoux, and W. Saxton. 2001. Spindle dynamics and the role of gamma-tubulin in early *Caenorhabditis elegans* embryos. *Mol. Biol. Cell.* 12:1751–1764.

Sullivan, D.S., and T.C. Huffaker. 1992. Astral microtubules are not required for anaphase B in *Saccharomyces cerevisiae*. *J. Cell Biol.* 119:379–388.

Verlhac, M.H., C. Lefebvre, P. Guillaud, P. Rassinier, and B. Maro. 2000. Asymmetric division in mouse oocytes: with or without Mos. *Curr. Biol.* 10:1303–1306.

Waters, J.C., T.J. Mitchison, C.L. Rieder, and E.D. Salmon. 1996. The kinetochore microtubule minus-end disassembly associated with poleward flux produces a force that can do work. *Mol. Biol. Cell.* 7:1547–1558.

Yang, H.Y., K. McNally, and F.J. McNally. 2003. MEI-1/katanin is required for translocation of the meiosis I spindle to the oocyte cortex in *C. elegans*. *Dev. Biol.* 260:245–259.

Yang, H.Y., P.E. Mains, and F.J. McNally. 2005. Kinesin-1 mediates translocation of the meiotic spindle to the oocyte cortex through KCA-1, a novel cargo adapter. *J. Cell Biol.* 169:447–457.